Potential effects of coagulation processes on phytoplankton mortality in the Elbe estuary from a Lagrangian point of view

Laurin Steidle[1], Johannes Pein, Adrian Burd, Ross Vennell

[1] *laurin.steidle@uni-hamburg.de*

Universitaet Hamburg, Grosse Elbstrasse 133, Germany

October 15, 2024

Abstract

Within the Elbe estuary, a sudden change in depth occurs when the river enters the shipping channel in the Port of Hamburg. This change in depth correlates with a sharp decline in phytoplankton concentrations. This decline affects the estuarine food web and shifts the ecosystem from autotrophic to heterotrophic during the summer months. Previous studies have hypothesized that this collapse is primarily driven by zooplankton grazing. We question this narrative and investigate the effect of phytoplankton aggregation with inorganic suspended matter and its impact on light limitation. In this study, we present a novel individual-based Lagrangian model to investigate the influence of aggregation on phytoplankton mortality. By incorporating data from the hydrodynamic model SCHISM and the sediment transport model SediMorph, we perform a Langragian simulation of the movement and aggregation of phytoplankton in the estuary. Our results show that aggregation with inorganic particles significantly increases sinking rates, leading to increased light limitation-induced mortality of phythoplankton, suggesting that aggregation processes may play an important role in explaining the collapse of phytoplankton concentration.

Introduction

Estuaries are typcially highly productive ecosystems and contribute disproportionately to the global carbon cycle, in addition to their role as a source of nutrients and breeding or hatching grounds for marine ecosystems (Cloern et al., 2014; Arevalo et al., 2023). They are also heavily influenced by anthropogenic stressors such as diking, dredging and fishing, and are of enormous importance for anthropogenic use (Jennerjahn and Mitchell, 2013; Brown et al., 2022; Wilson, 2002). Modern ecosystem management must balance the long-term sustainability of the ecosystem and climate with the economic interests of stakeholders.

The Elbe estuary is a particularly challenging example. Unlike other major European ports, the Port of Hamburg is located well inland, approximatelly 100 km from the coast. In order to provide access to the port for the largest class of container ships, the main channel experiences a sudden jump in bathymetry from about 5 m at the edge of the city to about 20 m in the harbour and downstream (see Fig. 1). This bathymetric jump is thought to be the main cause of the phytoplankton collapse (Schroeder, 1997; Schöl et al., 2014; Holzwarth et al., 2019; Pein et al., 2021).

The Elbe estuary is located in northern Germany and flows into the North Sea. Like most alluvial estuaries, it is relatively shallow near the sea, with an average depth of only a few metres in most parts. Like other European estuaries, it has been subject to strong anthropogenic pressures over the last century. In particular, dykes for land reclamation and flood protection have confined the Elbe to a narrow channel, and dredging to improve access to the port of Hamburg. Since 1900, the navigational channel has been dredged nine times from a depth of 7 m, most recently to 18 m in 2020. Ongoing dredging is also carried out to maintain the depth of the navigational channel. The increase in depth and the ongoing dredging are suspected to be the drivers for the increase in measured turbidity (Weilbeer et al., 2021; Kappenberg and Grabemann, 2001). While important aspects of the biochemical dynamics along the channel have been studied, little is known about their vertical and cross-channel or shore-to-shore dynamics (Goosen et al., 1999; Dähnke et al., 2008; Sanders et al., 2018).

Like most ecosystems, estuarine ecosystem dynamics are strongly controlled by primary producers, particularly phytoplankton, which form the basis of the estuarine food web (Chen et al., 2023).

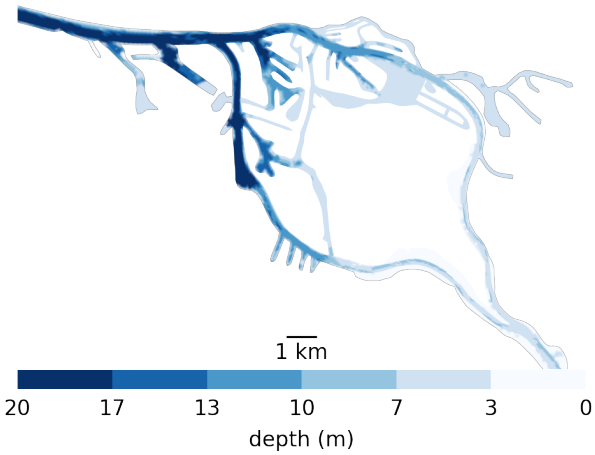

Figure 1: Bathymetry used in the Elbe model around Hamburg. Note, the bathymetry jumps from 5 m upstream (the right-hand side) to 10 m for a short step in the upper port area to 20 m in the lower port area all the way to the North Sea. Also note that there is only one channel to enter the harbor section of the estuary, which is mostly 20 m deep from shore to shore. So anything that passes through has to travel through deep water.

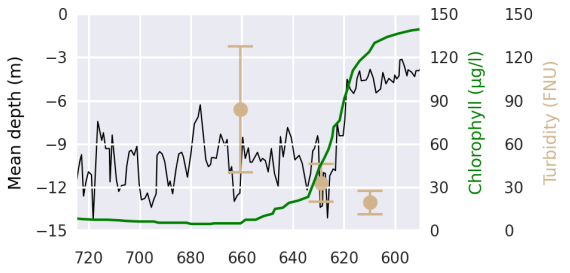

Figure 2: Chlorophyll concentrations as a proxy for phytoplankton biomass (green) and mean depth along a downstream transect averaged from shore-to-shore (black), showing the phytoplankton collapse and correlation with the bathymetric jump. Note, that the x-axis is inverted to keep consistancy with the map based plots. Data from (Schöl et al., 2014) and FGG-Elbe https://www.fgg-elbe.de/elbe-datenportal.html (last access: 3 March 2024) presenting the year 2012.

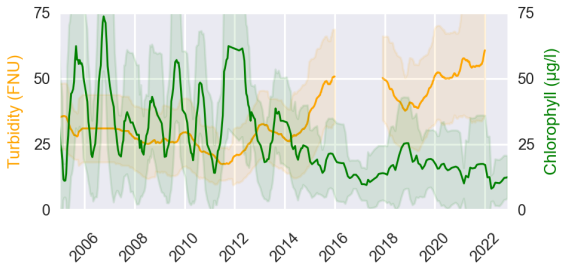

Figure 3: Chlorophyll concentraions as a proxy for phytoplankton biomass and turbidity. Measured from 2005 until 2023 at the station "Seemannshöft (Strom-km 628,9)" based on data open data available at FGG-Elbe https://www.fgg-elbe.de/elbe-datenportal.html (last access: 3 March 2024).

Apart from benthic biofilm-forming phytoplankton or microphytopbenthos (Cheah and Chan, 2022), the vast majority of phytoplankton organisms drift passively in currents.

Phytoplankton concentration drops suddenly in the harbour area of the estuary (see Fig. 2). The correlation with depth suggests that the collapse may be caused directly or indirectly by the bathymetric jump (Schroeder, 1997). Measurements of low oxygen concentrations (<3mg/l) and high ammonium ($15 mmol m^{-3}$) concentrations at the bottom and high disolved inorganic nitrogen downstream of the bathymetric jump suggest a high remineralisation rate of organic matter (Sanders et al., 2018; Spieckermann et al., 2022) which are consistent with model results (Schroeder, 1997; Holzwarth and Wirtz, 2018). This indicates that upstream phytoplankton is not being diluted or vertically dispersed in a way that allows it to elude the monitoring stations, but is actually dying. The collapse of the phytoplankton community also turns the estuary from a net autotrophic to a net heterotrophic system during the summer months (Schöl et al., 2014). Although this effect is well observed, the mechanisms behind this collapse are not well understood.

The collapse of the phytoplankton community in the Elbe estuary has been consistently observed in chlorophyll concentrations since the 1980s (Schöl et al., 2014). Looking at this trend over time we see that this effect has increased over recent years and is correlated with the increase in turbidity which has more then tripled since 2010 (Weilbeer et al., 2021) (see Fig. 3).

Most studies suggest that the phytoplankton collapse in the Elbe is due to grazing or light limitation. The *grazing hypothesis* assumes that most of the phytoplankton is consumed by zooplankton. A common explanation (Schöl et al., 2014; Hein et al., 2014; Pein et al., 2019) is that marine zooplankton are pushed into the estuary with the tides up to the

bathymetric jump. Upstream of the bathymetric jump, the flow velocity is much higher, making it difficult for them to migrate further upstream. This could explain the sudden drop in phytoplankton concentration in this area. Although marine zooplankton species have been observed in this area, (Steidle and Vennell, 2024) showed that retention in this area without a sophisticated mechanism is difficult for planktonic organisms. Hence, an accumulations of marine zooplankton to large enough concentrations that could explain this drop in chlorophyll concentrations might not be possible. This suggest that the grazing hypothesis might instead be dependant on upstream freshwater zooplankton that could still easily survive in the low salinity port area. Alternatively, the grazing pressure could be in part due to benthic grazers. With much lower flow velocities close to the bed and a potential ability to hold on or even burry themselves in the sediments they would have a much easier time to persist in that area. Informal reports of there existance have been made but no systematic study has been performed to date to try and quantize their abundance.

The last zooplankton survey that could be used to examine the effect of zooplankton grazing has been performed in 1992 (Bernat et al., 1994) with a small unpublished survey mentioned in (Schöl et al., 2014). At that time the bathymetry was significantly different with a narrower navigational channel and a target depth of 13m instead of the current 18m (Hein and Thomsen, 2023). Additionally the upstream biochemistry has changed significantly since the collapse of the German Democratic Republic (GDR) with a drastic increase in water quality and a corresponding increase in in upstream chlorophyll concentrations (Adams et al., 1996; Matthies et al., 2006). This effectively leaves us in the dark about the current impact of grazing on the chlorophyll concentrations.

The *light limitation* hypothesis is based on the sudden increase in turbidity downstream of the bathymetric jump and the sharp decrease in mean downstream velocity and corresponding increase in residence time. This increase in turbidity in turn increased the aphotic to photic volume ratio, effectively reducing light availability for phytoplankton. Note that the turbidity in the navigational channel is so high that water at a depth of bewlow two meters is aphotic (below 1% of surface light). However, a 1D-modelling study by (Schroeder, 1997), and the light limitation induced mortility rates measured by (Walter et al., 2017) suggest that light limitation alone would be too slow to explain the sudden drop in phytoplankton concentrations around the bathymetric jump. Instead, it could be explained with a combination of light limitation, grazing, and the sharp decrease in dowthnstream velocity. While light limitation restricts most of the phytoplankton growth, the decrease of the downstream velocity drastically increases residence times around the bathymetric jump. Combining this with an grazing pressure from upstream zooplankton could cause the sudden drop of the phytoplankton community. Typically chlorophyll concentrations are presented relative to the position along the channel obscuring the shift in residence times between these to regions which might in part explain the perceived suddenes of this effect. Another process considered in some models is referred to as *sedimentation* (Hagy et al., 2005; Iversonl et al., 2000). This is based on the assumption that individuals in the phytoplankton community have, on average, negative buoyancy. Therefore, they slowly sink, where some of them are assumed to be buried in the sediment. This process is also implemented in two Elbe models presented in (Schöl et al., 2014; Pein et al., 2021). However, this process lacks calibration and validation data in both models and with their choice of sinking losses are considered negligible compared to grazing losses.

Aggregation-induced-mortaility hypothesis

We suggest another explanation that has not yet been explored. Phytoplankton are typically thought to be sticky due to their excreted polysaccharides or transparent exopolymer particles (TEP) (Passow et al., 1994; Logan et al., 1995). If the suspended inorganic matter causing the high turbidity were to aggregate with the upstream phytoplankton, it would increase their sinking velocity. An increase in sinking velocity would shift their vertical distribution to deeper and henceforth darker waters. This in turn would increase light limitation effects and amplify the losses due to light limitation described above. A deeper average in the vertical column also reduce the downstream velocity as velocities towards the bottom are much lower and

may even flow upstream (Pein et al., 2021) further skewing the speed of the collapse after the batymetric jump when measured relative to the along channel position rather then residence time. The phytoplankton aggregates would also be more likely to settle to the bottom, further increasing their residence time, while creating an additional loss term due to potential benthic grazing. We therefore suspect that this *turbidity induced sinking* may be an important factor in the recent increase in the collapse of the phytoplankton community in the Elbe estuary.

Similar *aggregation and settling* processes, sometimes also referred to as flocculation and percipitation, have already demonstrated in lab studies (Deng et al., 2019) and observed in the North sea on the border between Wadden Sea and North Sea (Schartau et al., 2019; Neumann et al., 2019) The North Sea typically shows high organic aggregates concentrations while the Wadden Sea aggregates shows to be high in inorganic content. At their boundary hisometimes also referred to as flocculation and percipitation, gh precipitation can be observed, which is thought to be due to the aggregation of organic and inorganic particulates, which increases their sinking rate.

Particle aggregation in marine environments is a complex topic with many open questions. It is best researched in the context of open oceans where marine snow is a major pathway in the global carbon cycle and part of global climate forecasting models (Burd and Jackson, 2009; Jackson and Burd, 2015). First advances have been made studying phytoplankton coagulation in coastal environments (Chen and Skoog, 2017; Horemans et al., 2021) while most studies focus on inorganic sediments compared to the organic focus of open ocean models (Weilbeer et al., 2021; Cox et al., 2019). Aggregates in different environments differ drastically in their size distribution and composistion which in turns strongly effects their characteristics like shape, density, stickiness, and settling velocities making it hard to genererallize aggregation processes (Kriest, 2002; Cael et al., 2021; Laurenceau-Cornec et al., 2020).

The most common modelling approaches are from an Eulerian perspective where aggregates are modeled as concentration field for a set of aggregate size classes. Changes between these size classes are estimated using so called coagulation kernels (Stemmann et al., 2004; Burd, 2013). This in turn allows for the estimation of a particle size distribution and vertical fluxes. These Eularian aggegation models have the same advantages and disadvantages as other Eularian models - most notably that trajectories or life histories of individual particles and individual based processes are not represented.

Recently, several studies have studied aggregation processes from a (semi-)Lagration perspective (Jokulsdottir and Archer, 2016). So far, no study has examined the aggregation processes in coastal or estuarine environments from a Lagrangian perspective. Until the development of the OceanTracker model (Vennell et al., 2021) this was computationally expensive and difficult to implement. While there has not been a Lagrangian model examining aggregation in the Elbe estuary there have been severel Eulerian models.

All current Elbe estuary models represtend phytoplankton mortality as a combination of a nonlinear grazing loss function and a linear "natural mortality" or respiration loss function. Light limitation mortality is indirectly represtented as a limitation function in the growth rate. Aggregation processes are not represented in any of the existing models. Furthermore, while several models include Zooplankton grazing (Pein et al., 2021; Schöl et al., 2014; Holzwarth et al., 2019) they also use zooplankton grazing a tuning parameter such that the modeled concentrations fit the observed trends. Hence, a inference on the grazing induced mortality is not possible by these models, even though it is claimed in several publication (Schöl et al., 2014; Hein et al., 2014; Pein et al., 2019).

We will present a novel model study that attempts to draw attention to this issue. With this model we will investigate the effect phytoplankton aggregation processes from a Lagrangian perspective to examine the impact of "turbidity induced sinking" and the resulting light limitation induced mortality on the phytoplankton population. Although we have the same limitation of validation data as the previous studies, we try to provide first estimates of the relative importance of these processes that can serve as a basis for future research.

Methods

Model description

Lagrangian model: We have further developed the individual-based Lagrangian model OceanTracker (Vennell et al., 2021) and applied it to the Elbe estuary, similar to (Steidle and Vennell, 2024). Particle tracking on unstructured grids was relatively computationally expensive until recently, when Vennell et al. (2021) improved the performance by two orders of magnitude to the current state of the art. Looking at the problem from a Lagrangian perspective offers several advantages. First, it allows us to reuse computationally expensive hydrodynamic models to model tracer-like objects. This is overall much faster by several orders of magnitude than recalculating the advection-diffusion equation for tracers in an Eulerian model. Second, because we simulate particles individually, we are able to observe their tracks. This makes the interpretation of our results not only intuitive, but also allows us to include individual-based properties and processes that cannot be represented, or only indirectly, in Eulerian models.

Hydrodynamic data: We use the hydrodynamic data from the latest validated SCHISM model of the Elbe estuary (Pein et al., 2021). This model uses a three-dimensional unstructured grid to represent the entire Elbe estuary from the weir at Geesthacht to the North Sea, including several side channels and the port area (see Fig. 4). The model provides us with a node-based mesh containing a range of information such as water velocity, salinity, water level and dispersion. The year represented in this dataset is 2012 with a temporal resolution of 1 hour and a dynamically varying spatial resolution with node spacing ranging from 5 to 1400 m with a median spacing of about 75 m.

Suspended particulate matter data: Suspended particulate matter data has been provided by the SediMorph model (Malcherek et al., 2005) developed by the German Federal Waterways Engineering and Research Institute (Bundesanstalt für Wasserbau, BAW). SediMorph is coupled to the hydrodynamic model UnTRIM and provides data on the concentration of suspended particulates for five different size classes (see table 1)

Sediment	$-log_2$[mm]	d [μm]
Fine sand	> 3	128 - 256
Very fine sand	> 4	64 - 128
Coarse silt	> 5	32 - 64
Medium silt	> 6	16 - 16
Fine silt	> 7	8 - 16
Very fine silt	> 8	4 - 8

Table 1: SediMorph size classes and their corresponding size ranges.

The data was provided based on simulations for the year 2016 as a monthly average with a horizontal resolution ranging from 10 to 1000 m. It is based on approximatelly 100.000 horizontal nodes covering both the Elbe and Weser with a constant 1 m vertical resolution. The data was interpolated to the SCHISM grid as depth averaged values using a barycentric interpolation for the horizontal layer.

In this study we continuously release phytoplankton aggregates representing a subset of the incoming upstream phytoplankton population at the weir in Geesthacht. We then examine how the population distributes throughout the estuary by following their trajectory and, most importantly, their cause of death. As we are primarily interested in their cause of death and the mechanism behind hit we will be ignoring many other biological processes like cell growth and division.

Phytoplankton mortality causes: Mortality is induced by one of the following three processes: high salinity, light-limitation or "dry-out" when phytoplankton aggregates are stranded on the shore for to long.

When particles are exposed to *high salinity* water above 20PSU, a mortality probability of 0.5% per minute is imposed. This threshold is chosen based on a range of the salinity tolerances of estuarine phytoplankton species presented in (von Alvensleben et al., 2016). This is only an approximation and salinity tolerances many estuarine phytoplankton species deviate from this. However, the main motivation for this choice is that most of the particles that die through this process have passed the isohaline for more than 12 hours, one tidal cycle, and are assumed not to return again through this isohaline. Anything outside the 20 PSU isohaline is not considered part of the estuary for the

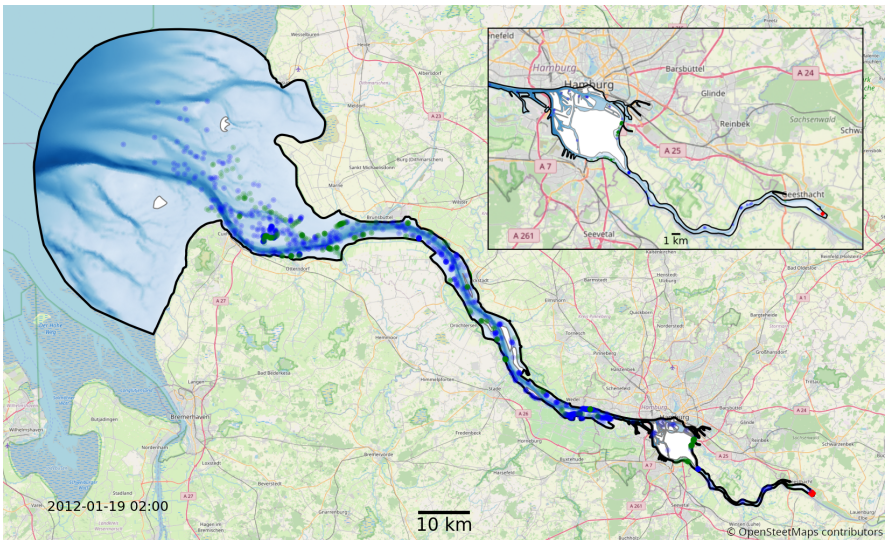

Figure 4: Map of the full model domain, with Geesthacht being the upstream boarder on the right and the North-sea being the downstream border on the left. The black outline marks the edge of the model domain. Blue and green dots show an example snapshot of a fraction of the phytoplankton in the model. The location of the initial release is shown in red. Blue represents floating, green particles stranded by the receding tide. The red area is the initial release location. The background map has been provided by © OpenStreetMap contributors 2023. Distributed under the Open Data Commons Open Database License (ODbL) v1.0.

purposes of this study. Therefore, we are not tailoring our salinity tolerance to a specific species, but rather testing whether they can retain themselves within this isohaline. This salinity induced mortality also allows us to reach a steady state population size, required to compare upstream and downstream populations easily.

We consider phytoplankton cells that were *stranded* out of the water by the receding tide and have lain dry for more than 7 consecutive days to be dead. Note that these dry cells are not typically devoid of water, but they are considered "dry" if the majority of their area has a water level below 0.1 m. Additionally, in nature, these areas typically contain small sub-resolution structures such as tidal ripples or small puddles and vegetation that allows these areas to remain wet for periods longer than one tidal cycle.

Light limitation is modelled based on observations presented in (Walter et al., 2017). They showed that phytoplankton can survive for several days with little or no light before the population starts to decline. To represent this, we model phytoplankton cells with a light budget. This light budget is represented as a moving average of their past illumination. Illumination is calculated once a minute at their current water depth. (Walter et al., 2017) showed that cell number growth rates during illumination and cell number death rates during darkness differ by about an order of magnitude. To compensate for this, we calculate the light budget using the maximum of two moving averages. The moving average ($\overline{I}$) of the local irradiance I_a at step $t+1$ is calculated by

$$\overline{I}(I,T)_{t+1} = \overline{I}(T-dt)_t + \frac{I_a(t)}{T} \qquad (1)$$

which allows them to recover from light limitation faster than they are starved of light. T is the averaging time and dt is the time step between averages. The light budget is then calculated as

$$LB = max(\overline{I}(I,T_g), \overline{I}(I,T_d)) \qquad (2)$$

where T_d is set to 12 days and T_g is set to 1/10 of T_d.

When the light budget falls below a threshold of $30\,\mathrm{W\,m^{-2}}$, the cells are considered light-limited and die with a probability of approximately $3.5 \times 10^{-5}\,\mathrm{min^{-1}}$ (Walter et al., 2017). The sensetivity of this threshold is examined in a sensetivity analysis presented in Sec. .

The surface light intensity or irradiance is modelled using the pvlib library (Anderson et al., 2023). We use pvlib to calculate the irradiance field based on the position of the sun relative to the location and time of year, assuming a clear sky.

The surface irradiance is then attenuated by the turbidity of the water column using the Beer-Lambert law.

$$I(z) = (1 - \alpha_a) I_0 e^{-\epsilon c z} \tag{3}$$

where $I(z)$ is the irradiance at depth z, I_0 is the surface irradiance, α_a is the surface albedo, ϵ is the attenuation coefficient, c is the turbidity based on the SPM concentration and z is the depth. The surface albedo is set to 0.1 and the chosen attenuation coefficient is 0.15 m^{-1}.

Aggregation induced buoyancy changes: We represent turbidity induced buoyancy by estimating particle collision and coagulation rates between the phythoplankton cells and the suspended particulate matter.

Typically three processes are considered when representing aggregation processes between organic and inorganic particles in marine environments: differential sedimentation, turbulent shear, and Brownian motion. Brownian motion can be neglected in our case because its effect is several orders of magnitude smaller for the size classes that we are considering. Differential sedimentation represents the potential for particles to aggregate based on different settling velocities causing relative motion between the particles, causing them to potantially collide. Turbulent shear represents the potential of particles to aggregate based on relative motion due to shear or small scale turbulences. We refer to these coagulation processes as different coagulation kernels These kernels can be represented in a rectilinear or curviliniear way. The later accounts for particles avoiding each other due the changes in the local flow field that the particles themselves cause while the first does not. The curviliniear kernels for turbulent shear β_{sh}^C and differential sedimentation β_{ds}^C are defined by

$$\beta_{sh}^C = (\frac{8\pi\epsilon}{15\nu})(1 - \frac{1 + 5p + 2.5p^2}{(1+p)^5})(r_i + r_j)^3 \tag{4}$$

$$\beta_{ds}^C = \frac{1}{2}\pi r_i^2 |v_i - v_j| \tag{5}$$

where ϵ is the turbulent kinetic energy dissipation rate, ν is the kinematic viscosity of the fluid, p is the particle size ratio r_i/r_j, r_i and r_j are the radii of the particles, v_i and v_j are the sinking velocities of the particles. Turbulent kinetic energy dissipation rate and kinematic viscosities are calculated and provided by the SCHISM model.

Estimating particle sinking velocities for aggregated particles is difficult as particle shape, size, and density can vary significantly between different aggregates. The classical approach using the Stokes law, which assumes that aggregates are spherical and homogeneously dense been show to be inadequate for complex marine aggregates as it drastically overestimates the sinking velocities (Kriest, 2002; Cael et al., 2021; Laurenceau-Cornec et al., 2020). Data availability for aggregates composition and size distritbution is typcially limititing in coastal environments that makes it difficult to apply tailord models. For our case we chose to use an empirical model presented by Kriest (Kriest, 2002). Here sinking velocities are calculated based on a power law and the fractal radius. Whilst there are many other potential models to represent the sinking velocities of aggregates, we found this to be the most suitable as it has been successfully applied in a modeling study already (Kriest, 2002) and because it is tuned to best represtend dense phytoplankton-based aggregates.

Sinking velocities are calculated using

$$v_i(d) = B d^{\nu} \tag{6}$$

d is the diameter of the aggregate, B and ν are fitting constants. Based on the "dense Phytoplankton aggregation model" (dPAM) presented in Kriest they are set to $942 d^{1.17}$ $\mathrm{m\,d^{-1}}$.

We assume that aggregates are sticky due to their exudates. This makes their stickiness proportional to the organic content. We therefore model the stickiness using the ratio of organic to inorganic content presented in (Jokulsdottir and Archer, 2016). The total particle coagulation rate is then calculated by

$$\beta = \alpha_s \frac{V_o}{V_i} (\beta_{sh}^C + \beta_{ds}^C) \tag{7}$$

where α_s is the maximum sticking probability of particles upon collision for a completely organic aggregate, V_o and V_i are the volumes of organic and

inorganic content in each aggregate, and β_{sh}^{C} and β_{ds}^{C} are the curvilinear coagulation kernels for turbulent shear and differential sedimentation. The amount of individual coagulations for each time step is then calculated based on the coagulation probabilities using a Poisson distribution.

Aggregate radius after collision is calculated assuming volume conservation

$$r_a^{t+1} = (r_a^3 + n r_{SPM}^3)^{1/3} \tag{8}$$

where r_a is the radius of the aggregate, r_{SPM} is the radius of the SPM particle, and n is the number of SPM particles that collided with the aggregate.

Settling and resuspension: We include a settling and resuspension model to represent tidal stranding and particles settling on the bed of the estuary. Particles become stranded when the current grid cell becomes dry. They are not allowed to move from wet cells to dry cells, by the random walk dispersion applied to all particles. A grid cell is considered dry based on the flag given in the SCHISM hydrodynamic model output. Once this cell is rewetted all stranded particles resuspend and are able to move again. Particles settle on the bed once they attempt to move below the bottom model boundary and are resuspended based on a critical sheer velocity of 0.009 ms^{-1} (see appendix for details). The velocity profile in the bottom layer, or log layer, is calculated by

$$U(z) = \frac{u_*}{\kappa} ln \frac{z}{z_0}, \tag{9}$$

where U is the friction velocity representing the drag at height z above the seabed, κ is the van Karman constant, z_0 is a length scale reflecting the bottom roughness, and u^* is the critical friction velocity. If the friction velocity is above the critical friction velocity the particle is resuspended.

Diffusivity: Particles are not only advected but also dispersed based on eddy diffusivity. This allows us implement a dynamic dispersion that is crucial to represent tidal-pumping processes. Dispersion was modeled using a random walk using a random number generator with a normal distribution. Horizontally the standard distribution of the random walk was set to 0.1 ms^{-1}. The displacement by vertical dispersion ∂z of particle i is calculated by

$$\partial z_i = K_v^{'}(z_i(n))\partial t + N(0, 2K_v(z_i)) \tag{10}$$

based on (Yamazaki et al., 2014) where z_i is the vertical position of the particle, $K_v^{'}$ is the vertical eddy diffusivity gradient, K_v is the vertical eddy diffusivity provided by the SCHISM model and N is the normal distribution. The term based $K_v^{'}$ is needed to avoid particle accumulation on the top and bottom of the water column from the hydrodynamic model output.

Technical details: For each particle we log their distance traveled, age, water depth, and status (whether they are drifting or settled on the river bank or bottom). These observables are recorded every 12 hours starting at midnight.

Model simulations and visualizations were performed in Python making heavy use of Numba, a LLVM-based Python JIT compiler (Lam et al., 2015) to significantly speed up the simulations (Vennell et al., 2021). Trajectories were calculated using a second order Runge-Kutta scheme with a fixed time step of 60 seconds. Flow velocities, like any other hydrodynamic data, were interpolated linearly in time and space using barycentric coordinates, with the exception of water velocity in the bottom model cell, where logarithmic vertical interpolation is used.

Experimental configurations

Conceptually, we run two kind of experimental setups, one with aggregation and one without. These experiments are accompanied by a series of sensitivity analyses to compensate for the lack of calibration data.

We model our population for a period of 1 year. The choice of 1 year is considered reasonable because it covers the full seasonal cycle and is also much longer than the average exit or flushing time of the estuary (see Fig. 10). We release 10 individuals per minute for one year at the weir in Geesthacht, resulting in approximately 5 million individuals per case, with approximately 50,000 individuals simultaneously alive. This corresponds to an approximate 1:1 ratio of simulated phytoplankton cells to mesh nodes in the hydrodynamic model at each time step. The released individuals are homogeneously distributed in a volume covering the

entire water column at the Geesthacht weir (bottom right in Fig. 4).

We also perform a number of sensitivity analyses to account for a lack of validation data. Most importantly, we test a range of different coagulation rates by tuning the sticking probability between 0 and 1 in steps of 0.1. We also test a range of light limitation induced mortality rates by tuning both the required average illumination threshold between 10W and 100W and a mortality rate between 0.03% and 0.0003% per minute when below this threshold.

We will compare the model using two metrics. As we are using a Lagrangian model, we can track the fate of each individual particle, in particular its cause of death. To compare the relative importance of the different mortaility causes, we compare the relative amount of aggregates dying to each of them for different model configurations, e.g. with and without aggregation.

The second metric use is the horizontal distribution of locations at which the death orccured. To visualize these we divide the model domain into equally sized hexagons. The color of each hexagon indicates the amount of phytoplankton aggregates that have died off in that particular bin. We use these to compare the along-stream alignment of the location of death to the observed oxygen minimum zone which is generally considered to be cause by the degradation and remineralization of the dead upstream phytoplankton. For this metric we will present the results for a stickiness of 1 for reasons presented in the discussion section.

Computations were performed on the supercomputer Mistral at the German Climate Computing Center (DKRZ) in Hamburg, Germany. The simulations were performed on a compute node with two Intel Xeon E5-2680 v3 12-core processor (Haswell) and 128 GB of RAM with a total run time of approximately 4 hours.

Results

Figure 5 and 6 shows the relative cause of death for a range of sticking probabilities. A a sticking probability α_s of zero represents the case without aggregation. In the following we will present the results observed throughout the summer months (April-September) while assuming initial aggregate diameters of 10,50 and 100 µm while focusing on the 50 µm case as the default. In the appendix Sec. and we are examining the sensetivity regarding the light limitation parameterisation.

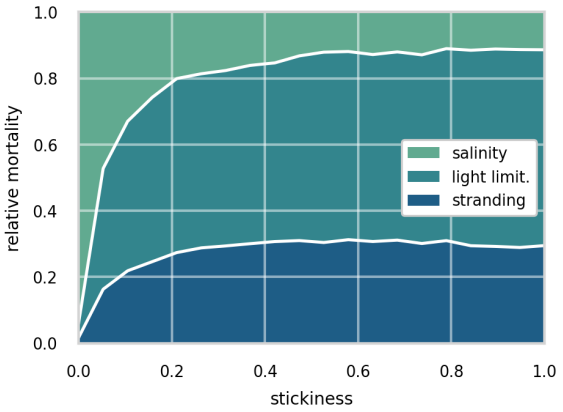

Figure 5: Relative cause of death for a range of stickiness parameterisations for an initial aggregate size of 50 µm.

For the 50 µm non-aggregation case (see Fig. 5), i.e. stickiness of zero, the main cause of death is salinity with losses due to light limitation around 4% while losses due to stranding are around 1%. Implying that most particles are advected out of the estuaries 20PSU isohaline. With an increase in sticking probability, we see a shift in the cause of death towards light limitation. For a sticking probability of 0.2, light limitation increases to around 53% and finds it maximum around 60% when the sticking probability is set to 1. With an increase in sticking probability, we also see an increase in the relative importance of stranding. Starting at around 1% for the non-aggregating case, it increases to around 28% for a sticking probability of 0.2 and remains that that level for a sticking probability of 1.

Comparing the 50 µm case to the 10 µm and 100 µm cases (see Fig. 6), we see a large sensetivity to the initial aggregate size. The importance of light limitation increases quickly with inital aggregate size. For the 10 µm case, light limitation induced mortality is below 20% for all sticking probabilities with salinity induced mortality causing 80% of deaths. Also, note the slow increase in light-induced mortality with increasing sticking probability, compared to the 50 µm or 100 µm cases, rising from approximately 4% at a sticking rate of 0 to just over 17% at a sticking rate of 1.

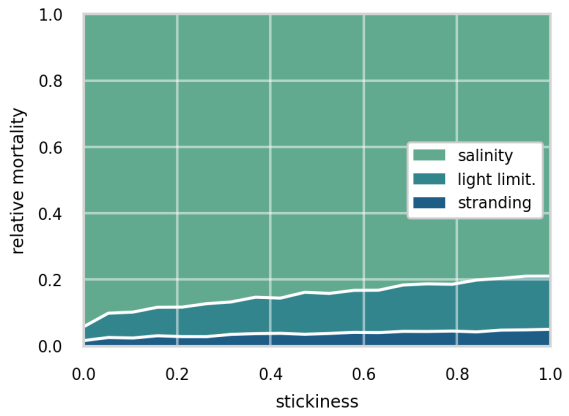

(a) 10 µm

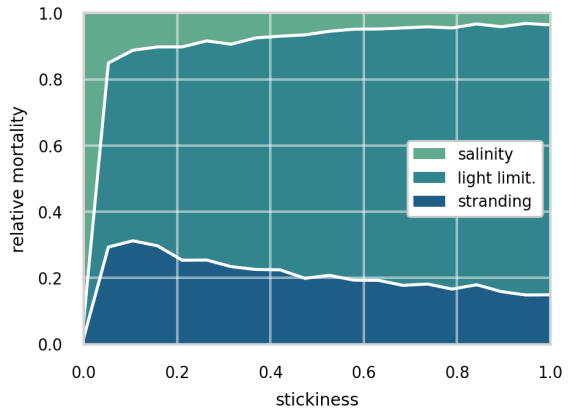

(b) 100 µm

Figure 6: Relative cause of death for a range of stickiness parameterisations for an initial aggregate size of a) 10 µm and b) 100 µm.

For the 100 µm case, light limitation induced mortality rapidly increases with sticking probability, reaching over 80% of the total mortality at a sticking probability of 1. For sticking probabilities over 0.1 we also see a decline in relative mortalities for stranding, something we do not see in the other cases, reaching its maximum at 0.1 sticking probabiliy with 30% of the total mortality and declining to 17% at a sticking probability of 1.

We now analyze the horizontal distribution of aggregate deaths with a hexagonal heatmap. Figure 7 shows the location of death for the non-aggregating and aggregating for the sommer months (April-September) for non-aggregating case (top) and for the aggregating case (bottom). Both presented cases assume an initial aggregate size of 50 µm and a stickiness of 1. The brightness of the collor in each hexagon indicates the relative amount of phytoplankton aggregates dying at that location. Note, the difference in scale between the two figures with the non-aggregation case ranging up to 1% and the aggregating case up to 12%. Hexagons where no aggregate died within the summer months are not colored.

Comparing the two, we see a clear shift in the location of death. For the non-aggregating case the main area of high mortality are located close to the mouth of the estuary with its peak close to Brunsbüttel. Note that this area coincides not only with a sharp increase in salinity but also in turbidity and ist often refered to as the maximum turbidity zone. A second but significantly less pronounced area of high mortality is located shortly after the bathymetric jump in both the Norder and Süderelbe.

For the aggregating case we see a shift in the location of death away from the maximum turbidity zone towards the bathymetric jump where where the majority - approximatelly 25% - of all aggregates die. A second area of high mortality is located close to the city Stade where two harbor bays seem to act as a sediment trap in our model. The previously observed area of high mortality around the turbidity maximum zone is now less pronounced. While it accounted for over 90% of the mortality in the non-aggregating case, it now accounts for less than 20% of the mortality in the aggregating case.

Taking a look at the outer end of the estuary, we also see a difference in the locations where no particles died. Notably, the tidal flats are largely empty of dead aggregates in the aggregating case, with almost all deaths occurring within the deeper sections of the estuary.

Interpretation and contextualization of the results

In this study, we examined the effect of aggregation processes on phytoplankton mortality in the Elbe estuary. Primarily, we focused on buoyancy changes due to aggregation with inorganic suspended particulate matter, which are suspected to increase mortality rates due to light limitation. We found that aggregation processes can significantly increase light limitation-induced mortality by over an order of magnitude (as shown in Fig.

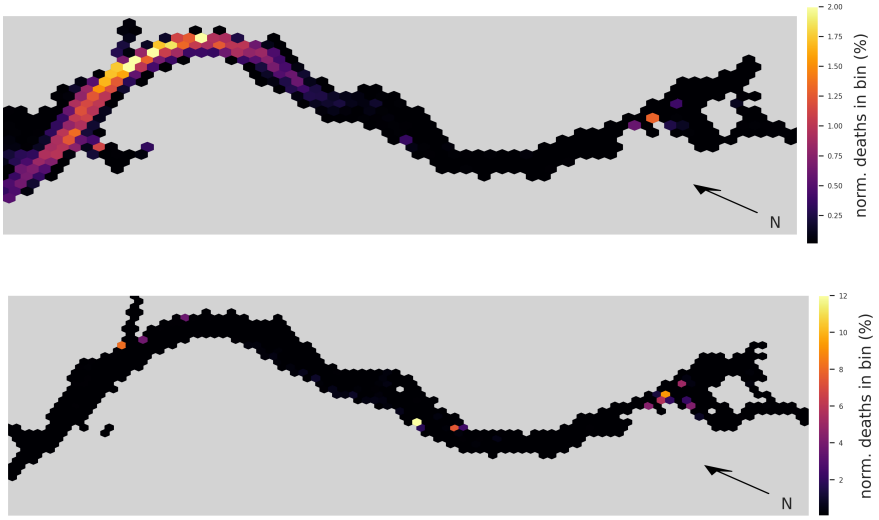

Figure 7: Hex-bin heatmap of the location of death for the summer months (April-September). The Hamburgs port area is located on the right with the North Sea to the left. Colors indicate the relative amount of phytoplankton aggregates dying at that location. The top figure represtens the non-aggregating case with yellowish colors indicating a loss greater than 1% of the community at that location, while the bottom figure represents the aggregating case with yellowish colors indicating a loss greater than 12% of the community at that location. Both caseses assume an initial aggregate size of 50 µm and a stickiness of one.

5). These results were consistent with observed changes in the location of death. The main location of death for phytoplankton aggregates, when accounting for buoyancy changes due to aggregation with suspended inorganic matter, was found to be shortly after the bathymetric jump. This finding is consistent with other studies examining the phytoplankton community from an Eulerian point of view (Pein et al., 2021; Schöl et al., 2014; Schroeder, 1997).

These results are also consistent with a recent taxonomic study by Martens et al. (2024). They showed that the large centric diatoms, which make up the majority of the upstream phytoplankton biomass, exhibit a negative correlation with the downstream position in the estuary. After the bathymetric jump, the composition shifts towards flagellates with the potential for mixotrophy and picophytoplankton (phytoplankton <3 µm in size), both of which have historically been underrepresented in microscopic studies. In the context of our study, the centric diatoms are typically in a size class represented by Fig. 6b, while the small picophytoplankton are in a size class represented by Fig. 6a. Hence, we suggest that the observed shift in the phytoplankton community composition might partly be explained by the increased light limitation-induced mortality of larger diatoms, the ability of mixotrophic flagellates to actively migrate within the water column, and their capacity to withstand darkness for longer periods due to their mixotrophic potential.

In our study we tested a range of sticking probabilities ranging from zero to one, i.e. from non-agreggating to always aggregating upon collision. Models representing aggregation that do not distinquish the content of aggregates typically work with sticking probabilities between 0.1 and 0.5 (Burd, 2013; Karakaş et al., 2009; Kriest, 2002), while the models that distinguishes between organic and inorganic content use a sticking probability of 1 (Jokulsdottir and Archer, 2016). Hence, we argue that for our case the sticking probability of 1 is the most realistic as well.

With the increase in depth, the volume for a cross-section segment increases significantly, which could lead one to conclude that the decrease in concentration is due to dilution. However, dilution requires mixing. In this case, it would require mixing the upstream high-chlorophyll freshwater with other low-chlorophyll waters. Because there are no significant tributaries that could dilute the up-

stream water with other freshwater, the only water that could mix with the upstream water is from the North Sea. While the North Sea water shows a lower chlorophyll concentration than the riverine water, it is also highly saline, with a salinity of above 30 PSU. Hence, any mixing is expected to be visible in the salinity concentrations. Because the collapse happens in a freshwater section of the estuary, with salinities of below 0.1 PSU, we do not expect dilution with seawater to account for the observed decrease in chlorophyll. However, our model design is currently not able to confirm this hypothesis.

Initially, we were surprised to observe how little light limitation contributed to mortality in the non-aggregating case. By examining the vertical velocities and locations of the aggregates, we found that they were traveling up and down the water column quickly, regularly reaching the surface where they could recover from light limitation. This is consistent with the general understanding of the Elbe estuary as a mostly "well-mixed" system. While the time spent at the surface is typically short and does not allow for much primary production, it seems to be sufficient to prevent light limitation-induced mortality in our model.

Model limitations & future perspectives

A major limitation of our study is the lack of grazing representation in our model. We would have liked to include a grazing model to directly compare the suggested light-limitation losses to grazing losses. This was not possible due to technical reasons within the time constraints of this study. Representing grazing losses would require an ecosystem model that tracks the zooplankton community and accounts for changes in, for example, the nutrient concentration field. This would necessitate an online particle tracking model that is directly coupled to the hydrodynamic model, which was too expensive both in terms of development time and computational resources. We hope that this study can motivate further work that includes an aggregation model into the existing Eulerian models to directly compare light limitation losses to grazing losses.

The lack of grazing in our model also limits us to making a weaker statement regarding the relative importance of light limitation losses compared to grazing losses. We are therefore not able to discuss the claim of (Schöl et al., 2014; Hein et al., 2014; Pein et al., 2019) that grazing is the main cause of phytoplankton losses in the Elbe estuary. We can only suggest that light limitation losses due to aggregation-enhanced sinking could be a significant cause of mortality.

Another limitation of our study is the uncertainty in the sinking velocities of the phytoplankton aggregates. As we highlighted in the methods section, the sinking velocities are based on a model by Kriest (Kriest, 2002). However, there are many other potential models to represent the sinking velocities of aggregates, as presented in (Cael et al., 2021; Laurenceau-Cornec et al., 2020). These different models can vary by an order of magnitude in their sinking velocities, making this a major source of uncertainty in our model. Additionally, these models are generally based on marine aggregates formed in significantly different environments than the Elbe estuary, most notably with much lower concentrations of suspended inorganic matter. We therefore assume that our sinking model is, in general, underestimating the sinking velocities of the phytoplankton aggregates, as the aggregates in the Elbe estuary are expected to be much denser than those in the open ocean. Thus, our estimates of the aggregation-induced light limitation losses are likely conservative.

The choice of coagulation kernel, whether to use a rectilinear or curvilinear kernel, also has a large effect on the effective coagulation rates. (Burd, 2013) compared the effects of these kernels on coagulation rates and showed that they can differ by several orders of magnitude, with the difference becoming more pronounced for larger aggregate size differences. See Sec. for a comparison of coagulation rates between these two kernels. Both kernels are analytically derived; however, a systematic comparison of these kernels in a real-world environment is missing. We chose to use the curvilinear kernels as they are generally assumed to be more accurate and also represent a more conservative estimate of the coagulation rates. Hence, our results of aggregation-induced light limitation losses are also a conservative estimate in that regard as well.

Another process that we neglect is the deaggregation of the phytoplankton aggregates. Shear and turbulence can cause the breakup of aggregates into smaller particles, which limits their size since they

are more likely to deaggregate the larger they become. This would be an interesting process to examine in our model, especially because we represent sinking speeds based on aggregate size. However, deaggregation is even less understood than aggregation, with next to no applicable data available. While some marine snow aggregation models include deaggregation processes, they represent them as fixed deaggregation rates or fixed upper size limits in a zeroth-order approximation (Burd, 2013; Karakaş et al., 2009; Jokulsdottir and Archer, 2016). Without data available to tune these rates, we decided to ignore this process in our model. We believe this to be reasonable as our aggregates are quickly growth-limited by Equation 7 and rarely exceed 1 mm in size.

We limit our aggregation model to inorganic particles exclusively. Hence, organic phytoplankton aggregates only aggregate with inorganic suspended matter. While this is a simplification, we believe it is justified by the difference in concentration between organic and inorganic particles. Particle concentration differences between organic and inorganic particles in the starting harbor, where most of the coagulation occurs, are around 1:1000. Assuming that they are of similar size, this also corresponds to a ratio in expected collisions of 1:1000, allowing us to ignore this process. Organic matter concentrations in the sediments of the channel are similarly low, with concentrations of less than 5% (Spieckermann et al., 2022). Aggregation processes can become strongly limited by the ratio of organic content in the larger aggregates, drastically reducing the sticking probability of aggregates with inorganic particulates, which could compensate for the difference in particle concentrations. Representing organic-to-organic aggregation would either require an online particle tracker that keeps track of the organic particle concentration or drastically increase the number of particles represented in the model (typical phytoplankton aggregate concentrations in nature can exceed million aggregates per cubic meter). Both options were infeasible, so we decided to ignore this process in our model.

We use hydrodynamic and SPM data representing the year 2012 and 2016 respectively. It would have been ideal to use data from the same year, but the two distingued models did not offer any overlapping years. While this represents an obvious inaccuracy we assume that this is justifiable as the bathymetriy did not change significantly between these years. To mask the natural variability between these datasets we used the SPM concentraions as monthly averages.

Outlook

We would like this study to be read as a proof of principle. We showed that aggregation processes can significantly increase light limitation-induced mortality in the Elbe estuary. Yet, we were not able to include grazing processes, which are currently assumed to be the major driver for phytoplankton community collapse. To achieve a better understanding of the relative importance of these processes, they would need to be integrated into a single model. This could be accomplished by either developing an interface between OceanTracker and SCHISM to enable online particle tracking or by implementing aggregation processes and size- and density-dependent buoyancy into existing Eulerian models. While the first approach would enable many interesting studies, it would also be more difficult to implement. The latter approach seems to be the simpler and more feasible way forward.

Another completely different approach to tackling this problem would be to gather zooplankton data. This would enable us to directly estimate filtration volumes and therefore grazing losses in the estuary, allowing us to evaluate the validity of the grazing hypothesis without a complex modeling study.

From an ecosystem management perspective, the abrupt collapse of the upstream freshwater phytoplankton community in the estuary is problematic because it leads to anoxic conditions, which in turn create an inhospitable environment for higher trophic levels, particularly fish. One approach to mitigating this problem is to enforce stricter regulations on fertiliser use in the upstream catchment, as high phytoplankton concentrations are largely due to eutrophication from agricultural fertiliser runoff (Holzwarth and Wirtz, 2018). Alternatively, reshaping the bathymetry of the estuary to ensure that community collapse occurs more gradually and further downstream, where larger surface-to-volume ratios and stronger vertical mixing can re-oxygenate the water more quickly.

We expect that issues related to turbidity will worsen in the future. Precipitation in Germany

is predicted to decrease (Huang, 2012), leading to lower discharge rates. With reduced upstream discharge, turbidity in the upper parts of the estuary, such as the harbour area, is expected to increase (Weilbeer et al., 2021). In addition, the expected sea level rise in the North Sea will increase tidal energy dissipation within the estuary, which will further increase turbidity due to increased vertical mixing (Pein et al., 2023). This has implications not only for local biota but also for sediment management costs in and around the shipping channel.

Acknowledgments

We thank the German Federal Waterways Engineering and Research Institute (Bundesanstalt für Wasserbau, BAW) for providing the crucial suspended particular matter data. LS acknowledges funding by the Deutsche Forschungsgemeinschaft (DFG, German Research Foundation) within the Research Training Group 2530: "Biota-mediated effects on Carbon cycling in Estuaries" (project number 407270017), contribution to Universität Hamburg and Leibniz-Institut für Gewässerökologie und Binnenfischerei (IGB) im Forschungsverbund Berlin e.V. JP acknowledges this study a contribution to Theme C of the Cluster of Excellence EXC 2037 'CLICCS - Climate, Climatic Change, and Society' - Project Number: 390683824 funded by the Deutsche Forschungsgemeinschaft (DFG, German Research Foundation) under Germany's Excellence Strategy.

Appendix

Sensitivity analysis on the light limitation culling threshold

Figure 8 presents a sensitivity analysis for the light limitation culling threshold. This threshold determines the average light input required over the past 12 days to prevent phytoplankton aggregates from dying due to light limitation (see Sec. **??**). We tested thresholds ranging from 10 to 100 $\mathrm{W\,m^{-2}}$ in increments of 5 $\mathrm{W\,m^{-2}}$.

Note that the threshold used in the main part of the study was 30 $\mathrm{W\,m^{-2}}$. The results indicate that this parameter is relatively insensitive compared to the initial aggregate size. However, doubling or halving the default light limitation culling threshold would cause the importance of light limitation as a cause of death to increase by about 20%, from 59% to 77%, or decrease by about 15%, from 59% to 44%, respectively.

We also observed that the relative changes in mortality causes diminish for larger thresholds, suggesting that this parameter becomes less sensitive at higher values.

The default threshold of 30 $\mathrm{W\,m^{-2}}$ is based on an assumed light compensation point of 10 $\mathrm{\mu mol\,m^{-2}\,s^{-1}}$, within a range of photosynthetically active radiation from 400 nm to 700 nm and a white light spectrum (Behrenfeld and Falkowski, 1997).

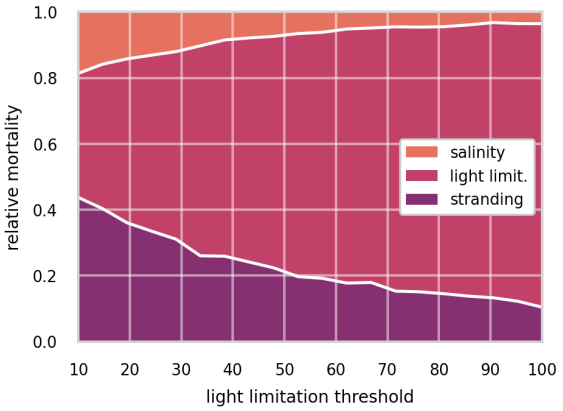

Figure 8: Relative cause of death for a range of light limitation thresholdes before inducing a mortality rate for an initial aggreage size of 50 µm.

Sensitivity analysis on the light limitation mortality rate

Figure 9 presents a sensitivity analysis for the light limitation mortality rate. This rate is applied to phytoplankton aggregates that have received, on average, less than 30 $\mathrm{W\,m^{-2}}$ of light in the past 12 days and is applied every 60 s (see Sec. **??**). We tested values ranging from one-tenth to ten times the default rate, i.e., from $3.56 \times 10^{-6}\,\mathrm{s^{-1}}$ to $3.56 \times 10^{-4}\,\mathrm{s^{-1}}$, in 20 steps of $7.19 \times 10^{-6}\,\mathrm{s^{-1}}$. The tested initial aggregate size is 50 µm with a stickiness factor of one. Note that while we are examining a range spanning two orders of magnitude, the data is presented with linear scaling to

maintain consistency with previous plots.

Our default value of $3.56 \times 10^{-5}\,\mathrm{s}^{-1}$ lies near a point of changing sensitivity. At this rate, the light limitation mortality ratio is approximately 60%. Reducing the light limitation mortality rate by a factor of 10 decreases this value to about 20%, while increasing it by a factor of 10 raises it to 80%. Halving the default value would reduce the light limitation mortality ratio to approximately 40%, while doubling it would increase the ratio to about 65%.

The chosen light limitation mortality rate is estimated based on an assumed exponential decay, as shown in the measurements presented by (Walter et al., 2017), where an average decline of 3% in cell numbers was reported after 12 days.

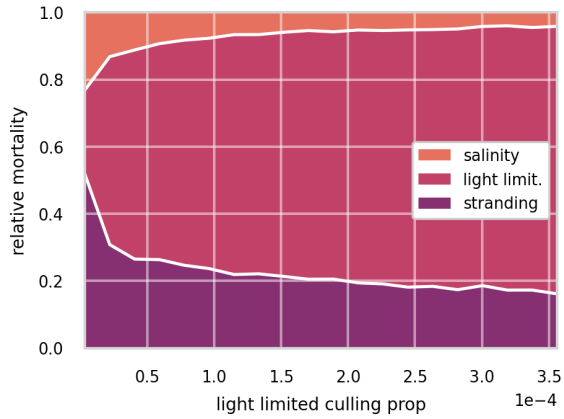

Figure 9: Relative cause of death for a range of light limitation mortality rates after falling below the light limitation threshold for an initial aggreage size of 50 µm

Sensitivity analysis on the coagulation kernel

Figure 11 compares the curvilinear coagulation kernel used in the study to a the simpler rectilinear kernel. We show the curvilinear kernel normalized to the rectilinear kernel for a range of partilce sizes from $1 \times 10^{-5}\,\mathrm{m}$ to $1 \times 10^{-3}\,\mathrm{m}$. Note, that the color scale is logarithmic, ranging from a ratio of 1/1000 to 1/10. As the curvilinear kernel accounts for particles avoiding each other due to the particle itself changing the flow in its proximity, effectively making particles avoid each other. Hence, the curvilinear kernels estimate smaller coagulation rates then rectilinear ones. For particles of equal size this effect reduces coagulation rates by approximatelly a factor of ten. For larger particle size differences this effects becomes more pronounced. Particles with a different in size of one order of magnitude have coagulation rates reduced by close two three orders of magnitude, while particles with a difference in size of two orders of magnitude have coagulation rates reduced by four to four orders of magnitude.

Hence, the choice between rectilinear and curvilinear kernels has an profound effect on the coagulation rates and consequently the relative importance of light limitation as a cause of death. While the curvilinear kernel are considered to me more accurate, the precise estimation of coagulations rates in a generalized form remains a challange (Burd, 2013). Nevertheless, as curvilinear kernels are strictly smaller then there rectilinear counterpart, they offer a conservative estimate on the importance of coagulation as a cause of death.

Flushing time

For comparison, the average exit time for water parcels to reach the 20 PSU isohaline per hexagon is shown in fig. 10. This calculation is based on a separate simulation where we released approximately 2 million particles homogeneously distributed over the estuary. We released one batch in winter during high discharge conditions on the first of January and another batch in summer during low discharge conditions at the first of July. Note, that for this simulation light-limitation, stranding and settling on the riverbed is disabled to isolate the effect of advection and dispersion.

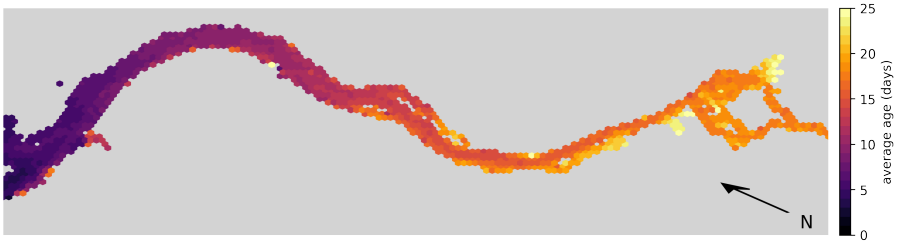

Figure 10: Hex-bin heatmap showing average exiting times of the Elbe estuary with Hamburgs port area, as shown in fig. **??**, on the right without reproduction, light-limitation, stranding and settling on the riverbed. Colors indicate the time of a water parcel to reach the 20 PSU isohaline from its origin hexagon.

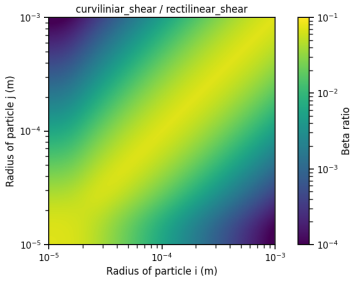

Figure 11: Comparison of the curvilinear coagulation kernel to the rectilinear kernel for a range of particle sizes. Note the logarithmic color scale.

References

Adams, M. S., Kausch, H., Gaumert, T., and Krüger, K.-E.: The effect of the reunification of Germany on the water chemistry and ecology of selected rivers, Environmental Conservation, 23, 35–43, https://doi.org/10.1017/S0376892900038236, 1996.

Anderson, K. S., Hansen, C. W., Holmgren, W. F., Jensen, A. R., Mikofski, M. A., and Driesse, A.: pvlib python: 2023 project update, Journal of Open Source Software, 8, 5994, https://doi.org/10.21105/joss.05994, 2023.

Arevalo, E., Cabral, H. N., Villeneuve, B., Possémé, C., and Lepage, M.: Fish larvae dynamics in temperate estuaries: A review on processes, patterns and factors that determine recruitment, Fish and Fisheries, 24, 466–487, https://doi.org/10.1111/faf.12740, 2023.

Behrenfeld, M. J. and Falkowski, P. G.: A consumer's guide to phytoplankton primary productivity models, Limnology and Oceanography, 42, 1479–1491, https://doi.org/10.4319/lo.1997.42.7.1479, 1997.

Bernat, N., Kopcke, B., Yasseri, S., Thiel, R., and Wolfstein3, K.: TIDAL VARIATION IN BACTERIA, PHYTOPLANKTON, ZOOPLANKTON, MYSIDS, FISH AND SUSPENDED PARTICULATE MATTER IN THE TURBIDITY ZONE OF THE ELBE ESTUARY; INTERRELATIONSHIPS AND CAUSES, 1994.

Brown, A. M., Bass, A. M., and Pickard, A. E.: Anthropogenic-estuarine interactions cause disproportionate greenhouse gas production: A review of the evidence base, Marine Pollution Bulletin, 174, 113 240, https://doi.org/10.1016/j.marpolbul.2021.113240, 2022.

Burd, A. B.: Modeling particle aggregation using size class and size spectrum approaches, Journal of Geophysical Research: Oceans, 118, 3431–3443, https://doi.org/10.1002/jgrc.20255, 2013.

Burd, A. B. and Jackson, G. A.: Particle aggregation, Annual Review of Marine Science, 1, 65–90, https://doi.org/10.1146/annurev.marine.010908.163904, 2009.

Cael, B. B., Cavan, E. L., and Britten, G. L.: Reconciling the Size-Dependence of Marine Particle Sinking Speed, https://doi.org/10.1029/2020GL091771, 2021.

Cheah, Y. T. and Chan, D. J. C.: A methodological review on the characterization of microalgal biofilm and its extracellular polymeric substances, Journal of Applied Microbiology, 132,

3490–3514, https://doi.org/10.1111/jam.15455, 2022.

Chen, T. Y. and Skoog, A.: Aggregation of organic matter in coastal waters: A dilemma of using a Couette flocculator, Continental Shelf Research, 139, 62–70, https://doi.org/10.1016/j.csr.2017.02.008, 2017.

Chen, W., Guo, F., Huang, W., Wang, J., Zhang, M., and Wu, Q.: Advances in phytoplankton population ecology in the Pearl river estuary, Frontiers in Environmental Science, 11, 1–8, https://doi.org/10.3389/fenvs.2023.1084888, 2023.

Cloern, J. E., Foster, S. Q., and Kleckner, A. E.: Phytoplankton primary production in the world's estuarine-coastal ecosystems, Biogeosciences, 11, 2477–2501, https://doi.org/10.5194/bg-11-2477-2014, 2014.

Cox, T. J., Maris, T., Engeland, T. V., Soetaert, K., and Meire, P.: Critical transitions in suspended sediment dynamics in a temperate meso-tidal estuary, Scientific Reports, 9, 1–10, https://doi.org/10.1038/s41598-019-48978-5, 2019.

Dähnke, K., Bahlmann, E., and Emeis, K.: A nitrate sink in estuaries? An assessment by means of stable nitrate isotopes in the Elbe estuary, Limnology and Oceanography, 53, 1504–1511, https://doi.org/10.4319/lo.2008.53.4.1504, 2008.

Deng, Z., He, Q., Safar, Z., and Chassagne, C.: The role of algae in fine sediment flocculation: In-situ and laboratory measurements, Marine Geology, 413, 71–84, https://doi.org/10.1016/j.margeo.2019.02.003, 2019.

Goosen, N. K., Kromkamp, J., Peene, J., Van Rijswijk, P., and Van Breugel, P.: Bacterial and phytoplankton production in the maximum turbidity zone of three European estuaries: The Elbe, Westerschelde and Gironde, Journal of Marine Systems, 22, 151–171, https://doi.org/10.1016/S0924-7963(99)00038-X, 1999.

Hagy, J. D., Boynton, W. R., and Jasinski, D. A.: Modelling phytoplankton deposition to Chesapeake Bay sediments during winter-spring: Interannual variability in relation to river flow, Estuarine, Coastal and Shelf Science, 62, 25–40, https://doi.org/10.1016/j.ecss.2004.08.004, 2005.

Hein, B., Viergutz, C., Wyrwa, J., Kirchesch, V., and Schöl, A.: Modelling the Impact of Climate Change on Phytoplankton Dynamics and the Oxygen Budget of the Elbe River and Estuary (Germany), Tech. rep., Bundesanstalt für Wasserbau, 2014.

Hein, J. and Thomsen, J.: Contested estuary ontologies: The conflict over the fairway adaptation of the Elbe River, Germany, Environment and Planning E: Nature and Space, 6, 153–177, https://doi.org/10.1177/25148486221098825, 2023.

Holzwarth, I. and Wirtz, K.: Anthropogenic impacts on estuarine oxygen dynamics: A model based evaluation, Estuarine, Coastal and Shelf Science, 211, 45–61, https://doi.org/10.1016/j.ecss.2018.01.020, 2018.

Holzwarth, I., Weilbeer, H., and Wirtz, K. W.: The effect of bathymetric modification on water age in the Elbe Estuary, 2019.

Horemans, D. M., Dijkstra, Y. M., Schuttelaars, H. M., Sabbe, K., Vyverman, W., Meire, P., and Cox, T. J.: Seasonal Variations in Flocculation and Erosion Affecting the Large-Scale Suspended Sediment Distribution in the Scheldt Estuary: The Importance of Biotic Effects, Journal of Geophysical Research: Oceans, 126, 1–20, https://doi.org/10.1029/2020JC016805, 2021.

Huang, S.: Modelling of environmental change impacts on water resources and hydrological extremes in Germany, Ph.D. thesis, Universitätsbibliothek der Universität Potsdam, 2012.

Iversonl, R. L., Landing, W. M., and Lewis, F. G.: Control of phytoplankton production and biomass in a river-dominated estuary: Apalachicola Bay, Florida, USA, 2000.

Jackson, G. A. and Burd, A. B.: Simulating aggregate dynamics in ocean biogeochemical models, Progress in Oceanography, 133, 55–65, https://doi.org/10.1016/j.pocean.2014.08.014, 2015.

Jennerjahn, T. C. and Mitchell, S. B.: Pressures, stresses, shocks and trends in estuarine ecosystems - An introduction and synthesis, Estuarine, Coastal and Shelf Science, 130, 1–8, https://doi.org/10.1016/j.ecss.2013.07.008, 2013.

Jokulsdottir, T. and Archer, D.: A stochastic, Lagrangian model of sinking biogenic aggregates in the ocean (SLAMS 1.0): Model formulation, validation and sensitivity, Geoscientific Model Development, 9, 1455–1476, https://doi.org/10.5194/gmd-9-1455-2016, 2016.

Kappenberg, J. and Grabemann, I.: Variability of the mixing zones and estuarine turbidity maxima in the Elbe and Weser estuaries, Estuaries, 24, 699–706, https://doi.org/10.2307/1352878, 2001.

Karakaş, G., Nowald, N., Schäfer-Neth, C., Iversen, M., Barkmann, W., Fischer, G., Marchesiello, P., and Schlitzer, R.: Impact of particle aggregation on vertical fluxes of organic matter, Progress in Oceanography, 83, 331–341, https://doi.org/10.1016/j.pocean.2009.07.047, 2009.

Kriest, I.: Different parameterizations of marine snow in a 1D-model and their influence on representation of marine snow, nitrogen budget and sedimentation, 2002.

Lam, S. K., Pitrou, A., and Seibert, S.: Numba : A LLVM-based Python JIT Compiler, https://doi.org/10.1145/2833157.2833162, 2015.

Laurenceau-Cornec, E. C., Moigne, F. A. L., Gallinari, M., Moriceau, B., Toullec, J., Iversen, M. H., Engel, A., and Rocha, C. L. D. L.: New guidelines for the application of Stokes' models to the sinking velocity of marine aggregates, Limnology and Oceanography, 65, 1264–1285, https://doi.org/10.1002/lno.11388, 2020.

Logan, B. E., Passow, U., Alldredge, A. L., Grossarts, . H.-P., and Simon+, M.: Rapid formation and sedimentation of large aggregates is predictable from coagulation rates (half-lives) of transparent exopolymer particles (TEP), 1995.

Malcherek, A., Piechotta, F., and Knoch, D.: Mathematical Module SediMorph Validation Document-Version 1.1, Tech. rep., The Federal Waterways Engineering and Research Institute (BAW), 2005.

Martens, N., Russnak, V., Woodhouse, J., Grossart, H.-P., and Schaum, C.-E.: Metabarcoding reveals potentially mixotrophic flagellates and picophytoplankton as key groups of phytoplankton in the Elbe estuary, Environmental Research, 252, 119 126, https://doi.org/10.1016/j.envres.2024.119126, 2024.

Matthies, M., Berlekamp, J., Lautenbach, S., Graf, N., and Reimer, S.: System analysis of water quality management for the Elbe river basin, Environmental Modelling and Software, 21, 1309–1318, https://doi.org/10.1016/j.envsoft.2005.04.026, 2006.

Neumann, A., Hass, H. C., Möbius, J., and Naderipour, C.: Ballasted flocs capture pelagic primary production and alter the local sediment characteristics in the coastal German bight (North sea), Geosciences (Switzerland), 9, https://doi.org/10.3390/geosciences9080344, 2019.

Passow, U., Alldredge, A. L., and Logant, B. E.: The role of particulate carbohydrate exudates in the flocculation of diatom blooms, 1994.

Pein, J., Eisele, A., Hofmeister, R., Sanders, T., Daewel, U., Stanev, E. V., Beusekom, J. V., Staneva, J., and Schrum, C.: Nitrogen cycling in the Elbe estuary from a joint 3D-modelling and observational perspective, Biogeosciences Discussions, 2019, 1–34, https://doi.org/10.5194/bg-2019-265, 2019.

Pein, J., Eisele, A., Sanders, T., Daewel, U., Stanev, E. V., van Beusekom, J. E. E., Staneva, J., and Schrum, C.: Seasonal Stratification and Biogeochemical Turnover in the Freshwater Reach of a Partially Mixed Dredged Estuary, Frontiers in Marine Science, 8, https://doi.org/10.3389/fmars.2021.623714, 2021.

Pein, J., Staneva, J., Mayer, B., Palmer, M. D., and Schrum, C.: A framework for estuarine future sea-level scenarios: Response of the industrialised Elbe estuary to projected mean sea level rise and internal variability, Frontiers in Marine Science, 10, https://doi.org/10.3389/fmars.2023.1102485, 2023.

Sanders, T., Schöl, A., and Dähnke, K.: Hot Spots of Nitrification in the Elbe Estuary and Their Impact on Nitrate Regeneration, Estuaries and Coasts, 41, 128–138, https://doi.org/10.1007/s12237-017-0264-8, 2018.

Schartau, M., Riethmüller, R., Flöser, G., van Beusekom, J. E., Krasemann, H., Hofmeister, R., and Wirtz, K.: On the separation between inorganic and organic fractions of suspended matter in a marine coastal environment, Progress in Oceanography, 171, 231–250, https://doi.org/10.1016/j.pocean.2018.12.011, 2019.

Schöl, A., Hein, B., Wyrwa, J., and Kirchesch, V.: Modelling Water Quality in the Elbe and its Estuary – Large Scale and Long Term Applications with Focus on the Oxygen Budget of the Estuary, 81, 203–232, 2014.

Schroeder, F.: Water quality in the Elbe estuary: Significance of different processes for the oxygen deficit at Hamburg, Environmental Modeling and Assessment, 2, 73–82, https://doi.org/10.1023/a:1019032504922, 1997.

Spieckermann, M., Gröngröft, A., Karrasch, M., Neumann, A., and Eschenbach, A.: Oxygen Consumption of Resuspended Sediments of the Upper Elbe Estuary: Process Identification and Prognosis, Aquatic Geochemistry, 28, https://doi.org/10.1007/s10498-021-09401-6, 2022.

Steidle, L. and Vennell, R.: Phytoplankton retention mechanisms in estuaries: A case study of the Elbe estuary, Nonlinear Processes in Geophysics, 31, 151–164, https://doi.org/10.5194/npg-31-151-2024, 2024.

Stemmann, L., Jackson, G. A., and Ianson, D.: A vertical model of particle size distributions and fluxes in the midwater column that includes biological and physical processes - Part I: Model formulation, Deep-Sea Research Part I: Oceanographic Research Papers, 51, 865–884, https://doi.org/10.1016/j.dsr.2004.03.001, 2004.

Vennell, R., Scheel, M., Weppe, S., Knight, B., and Smeaton, M.: Fast lagrangian particle tracking in unstructured ocean model grids, Ocean Dynamics, 71, 423–437, https://doi.org/10.1007/s10236-020-01436-7, 2021.

von Alvensleben, N., Magnusson, M., and Heimann, K.: Salinity tolerance of four freshwater microalgal species and the effects of salinity and nutrient limitation on biochemical profiles, Journal of Applied Phycology, 28, 861–876, https://doi.org/10.1007/s10811-015-0666-6, 2016.

Walter, B., Peters, J., and van Beusekom, J. E.: The effect of constant darkness and short light periods on the survival and physiological fitness of two phytoplankton species and their growth potential after re-illumination, Aquatic Ecology, 51, 591–603, https://doi.org/10.1007/s10452-017-9638-z, 2017.

Weilbeer, H., Winterscheid, A., Strotmann, T., Entelmann, I., Shaikh, S., and Vaessen, B.: Analyse der hydrologischen und morphologischen Entwicklung in der Tideelbe für den Zeitraum von 2013 bis 2018, Die Küste, 89, 57–129, URL https://doi.org/10.18171/1.089104., 2021.

Wilson, J. G.: Productivity, fisheries and aquaculture in temperate estuaries, Estuarine, Coastal and Shelf Science, 55, 953–967, https://doi.org/10.1006/ecss.2002.1038, 2002.

Yamazaki, H., Locke, C., Umlauf, L., Burchard, H., Ishimaru, T., and Kamykowski, D.: A Lagrangian model for phototaxis-induced thin layer formation, Deep Sea Research Part II: Topical Studies in Oceanography, 101, 193–206, https://doi.org/10.1016/j.dsr2.2012.12.010, 2014.